Grain-size effects on the charge ordering and exchange bias in $Pr_{0.5}Ca_{0.5}MnO_3$: The role of spin configuration

T. Zhang and M. Dressel
1. Physikalisches Institut, Universität Stuttgart, Pfaffenwaldring 57, D-70550 Stuttgart, Germany
(Received 18 February 2009; revised manuscript received 16 June 2009; published 31 July 2009)

The grain-size effects on the charge ordering and exchange bias in CE-type antiferromagnetic charge ordered manganite compound $Pr_{0.5}Ca_{0.5}MnO_3$ are explored by magnetometry. Reducing the size suppresses antiferromagnetism and charge ordering that does not occur any more when the size is smaller than 40 nm. At the same time ferromagnetic clusters appear and gradually become larger; their fraction increases to about 19.7% when the particle size is reduced to 20 nm. The magnetic hysteresis loops of the nanosized samples exhibit both horizontal and vertical shifts in the field-cooled process. The exchange bias field H_{eb} and the coercivity H_C do not depend monotonously on size but show a maximum at about 85 nm, which indicates that in antiferromagnetic charge-ordered manganites H_{eb} can be effectively tuned by changing the grain size. These notable phenomena can be understood when the evolution of the spin configuration is considered that results from the surface-phase separation and surface effect.

DOI: 10.1103/PhysRevB.80.014435 PACS number(s): 75.47.Lx, 75.30.Et, 75.50.Tt

I. INTRODUCTION

Doped manganites with a perovskite structure $R_{1-x}A_xMnO_3$ (R and A being rare-earth and alkaline-earth ions, respectively) show a wide variety of magnetoelectronic phenomena such as colossal magnetoresistance, charge ordering (CO), and electronic phase separation on a nanoscale because of the strong coupling of the spin, charge, orbital, and lattice degrees of freedom and the intense competition between the ferromagnetic (FM) metallic and antiferromagnetic (AFM) insulating phases.[1–6] As a result, the ground state is dependent on which interaction dominates and it can be tuned not only by applied external fields and pressure but also by the geometrical and chemical environment at the surface of the system.[7–10] In nanosized materials the surface/volume ratio is large and, as a consequence, the surface effects play a crucial role, which has been observed in a series of recent experiments. For example, in materials where a FM state is stabilized in the bulk, an AFM or spin-glass surface state is found in nanoparticles.[11–15] For manganites with AFM/CO phases in the bulk, a FM component or FM clusters is observed at the surface of nanosized samples, at the same time the CO phase is significantly weakened.[2,16–21]

However, there is also some debate about manganites with AFM/CO ground state, for instance, Lu *et al.*[18] found that 20-nm-sized $La_{0.4}Ca_{0.6}MnO_3$ compound demonstrates FM-like ordering with spontaneous magnetization $M_S \sim 1\ \mu_B$/f.u. at $T=5$ K. Rozenberg *et al.*,[20] however, reported that AFM/CO state continues to exist in the same-sized compound and their value of $M_S \sim 0.0045\ \mu_B$/f.u. at $T=5$ K is much smaller than that by Lu *et al.*[18] In addition, it has been shown recently that for bulk $La_{0.9}Ca_{0.1}MnO_3$ compound with mixed magnetic ordering, the suppression of the inherent structural/chemical inhomogeneity results in a FM-like ground state in nanosamples,[22] while both bulk and nano-$La_{0.7}Ca_{0.3}MnO_3$ are FM state.[14]

In manganites, interactions of different types can be of comparable strengths, which leads to a great variability and complexity of their ground state. Therefore, the size effect on the magnetic properties and CO are far away from being clearly understood and their mechanism is subject of intense debate. Moreover, a Monte Carlo study has recently been performed on the CE-type AFM/CO phase in a three-dimensional lattice with an open surface; it revealed that an increase in charge density due to the unscreened Coulomb interactions drives the surface layer from an AFM/CO to a phase-separated state and provides the FM tendency at the surface,[23] while the inner core is still a stable CE-type CO state. This prediction needs to be confirmed by experiment.

Another interesting phenomenon is that at the interface of FM and AFM components in a certain material, exchange bias (EB) effect occurs when the FM-AFM system is cooled in a static magnetic field through the Néel temperature T_N of the AFM phase. The induced unidirectional anisotropy leads to a shift in the magnetization hysteresis loop, usually oriented opposite to the direction of the external field in which sample is cooled.[24] When we start from the AFM/CO bulk manganites and reduce their grain size to nanoscale, the FM component or FM clusters appear at the surface while the core is still a collinear AFM or a canted AFM. Thus, a natural FM/AFM interface appears that should lead to the intrinsic EB effect. The EB field is closely related to the thickness of the FM and AFM layers.[24,25] With reducing grain size, the ratio of FM shell and AFM core rises and the spin configuration changes significantly; this will lead to a variation in the EB field with grain size. Up to now, most experimental and theoretical studies of EB have been performed for FM-AFM multilayer and for FM nanoparticles embedded in an AFM matrix.[25] Only recently, EB effects were reported for the nanosized $La_{0.7}Ca_{0.3}MnO_3$ with a FM core and a spin-glass shell[26] and for the nanosized $La_{0.25}Ca_{0.75}MnO_3$ with FM clusters embedded in an AFM matrix.[27] But due to the complex phases of different manganite systems, the size effect on the EB field and its mechanism is not clearly understood.

The half-doped bulk manganite $Pr_{0.5}Ca_{0.5}MnO_3$ has a typical CE-type AFM/CO phase below $T=250$ K and the CO state is so stable that a magnetic field of $H=270$ kOe is

needed to melt it completely; this effect is strongly correlated with the collinear AFM ordering of the localized Mn moments.[10] Moreover, the CE-type magnetic structure is different with the coexistence of the CE- and C-type ones in $La_{0.25(0.4)}Ca_{0.75(0.6)}MnO_3$ compounds.[6] So studying nano-$Pr_{0.5}Ca_{0.5}MnO_3$ compound may lead to different phenomena compared to those in Refs. 2 and 20. Although recently, Sarkar *et al.*[21] presented the structure and transport results of nanosized $Pr_{0.5}Ca_{0.5}MnO_3$ and suggested that the size reduction reduces the cell volume and weakens the robust CO. However, the variation in the magnetic structure with grain size is not explored in detail and that exchange bias effect and its tune by grain size have not been reported in this nanocompound. In order to obtain more insight into the problem, the present investigation focuses on tuning the CO and the EB by grain size in $Pr_{0.5}Ca_{0.5}MnO_3$

II. EXPERIMENT

Polycrystalline nanoparticles of $Pr_{0.5}Ca_{0.5}MnO_3$ were prepared by a sol-gel method described in Ref. 2. X-ray diffraction (XRD) pattern of each sample confirmed that the crystals are in orthorhombic phase. The composition of all samples was checked by the inductively coupled plasma atomic-emission spectroscopy techniques; within the experimental uncertainty, the results are in agreement with the nominal composition (molar ratio of Pr:Ca:Mn=1:1:2). The oxygen stoichiometry was checked by $K_2Cr_2O_7$ and $FeSO_4$ titration for some typical samples with grain sizes 300, 70, and 20 nm, respectively. For each sample, this titration was performed three times. The results indicate that the three samples have almost the same oxygen content ($3-\delta$ with $\delta=0.016\pm0.003$). We conclude that this also holds for the other specimens. The magnetization measurements were performed using a superconducting quantum interference device magnetometer. The magnetic hysteresis loops were measured between $H=-50$ and 50 kOe after cooling the sample from 300 K to the measuring temperature in zero-field-cooled (ZFC) or field-cooled (FC) processes; the field for the FC process was $H=10$ kOe. The relaxation is measured after the sample was rapidly cooled in zero field from room temperature to the measuring temperature and was kept for different waiting time t_w. Then the relaxation of the magnetization was recorded as a function of the time elapsed after an application of a probing field $H=100$ Oe.

III. RESULTS AND DISCUSSION

The X-ray diffraction patterns confirm the single phase and crystallization nature of all the nanoparticles with orthorhombic crystal structure, as shown in Fig. 1. The average diameter D was estimated by the field-emission scan electron microscopy (FE-SEM) images [as shown in Figs. 2(a) and 2(b)] and Scherrer formulation $D=k\lambda/(\beta\cos 2\theta)$, where D is the diameter of the grain, k is a constant (0.9), λ is the wavelength of the x-ray, and β is the full width of the half maximum of a peak. As shown in Table I, D increases from 20 to 300 nm as the annealing temperature is increased from 500 to 1000 °C. The size distribution of the samples with

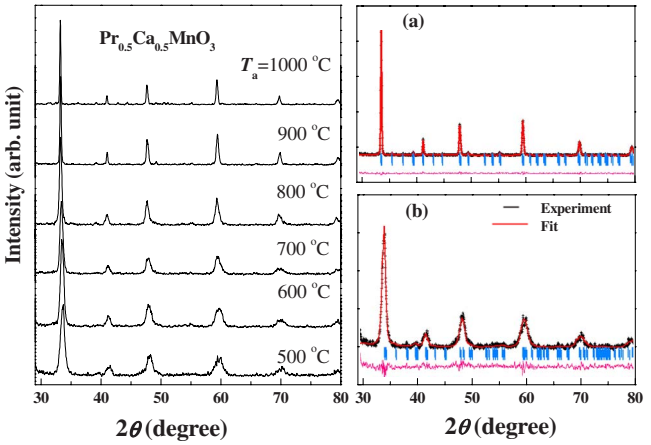

FIG. 1. (Color online) The x-ray diffraction patterns for the as-prepared $Pr_{0.5}Ca_{0.5}MnO_3$ samples at different annealing temperatures. Experiment (black cross) and Rietveld fitted (red solid line) XRD patterns for the samples with average grain size (a) 300 and (b) 20 nm. The magenta curve is the error.

average particle size of 20 and 300 nm was determined by FE-SEM [cf. Figs. 2(c) and 2(d)]; the width of size distribution of all samples is presented in Table I. The diffraction data are analyzed using the Rietveld profile-fitting program according to the orthorhombic space group *Pnma*.[28] The structure parameters listed in Table I reveal that the size reduction leads to a shrinkage of the cell volume, in agreement with the result by Rozenberg *et al.*[20,22] and Sarkar *et al.*[21]

Figure 3 shows the temperature dependence of the magnetization measured at $H=100$ Oe after FC and ZFC procedures. For $D=300$ nm, the magnetization increases with decreasing temperature below 300 K displaying a maximum at about 251 K that corresponds to the development of the CO state.[28] As the temperature is reduced further, the ZFC curve demonstrates another cusp at about 34 K, while the FC one continues to increase below this temperature. These finding are confirmed by Cao *et al.*[29] and Lees *et al.*[30] This behavior is ascribed to the reentrant spin glass (RSG),[29] where the onset temperature of RSG state T_{SG} is defined by the inflection point in the dM/dT versus T plot; the peak temperature at about 34 K in the ZFC curve is defined as the spin-freezing temperature T_f. The plot of the ac magnetization vs temperature at different frequencies supports the spin-glass state, as shown in the inset of Fig. 3(a). For $D=150$ nm, the peak corresponding to the CO transition becomes wide and shifts to a lower temperature (248 K) compared with $D=300$ nm. This behavior is better seen in the inset of the Fig. 3(c). In addition to the RSG state, at a slightly higher temperature ($T\sim70$ K) an upturn of the magnetization can be identified which we assign to the reappearance of the weak FM double exchange interaction; it can be seen in the inset of Fig. 3(b) as the weak inflection point of dM/dT vs T curve slightly above T_{SG}. The CO peak is significantly weakened for $D\leq85$ nm; the clear rapid increase in magnetization at higher temperatures ($T>70$ K) corresponds to the FM or FM cluster glass (CG) state transition. The signal of the spin glass faints due to the cover up by FM component or FM clusters. Below 70 nm, the characteristic of CO transitions

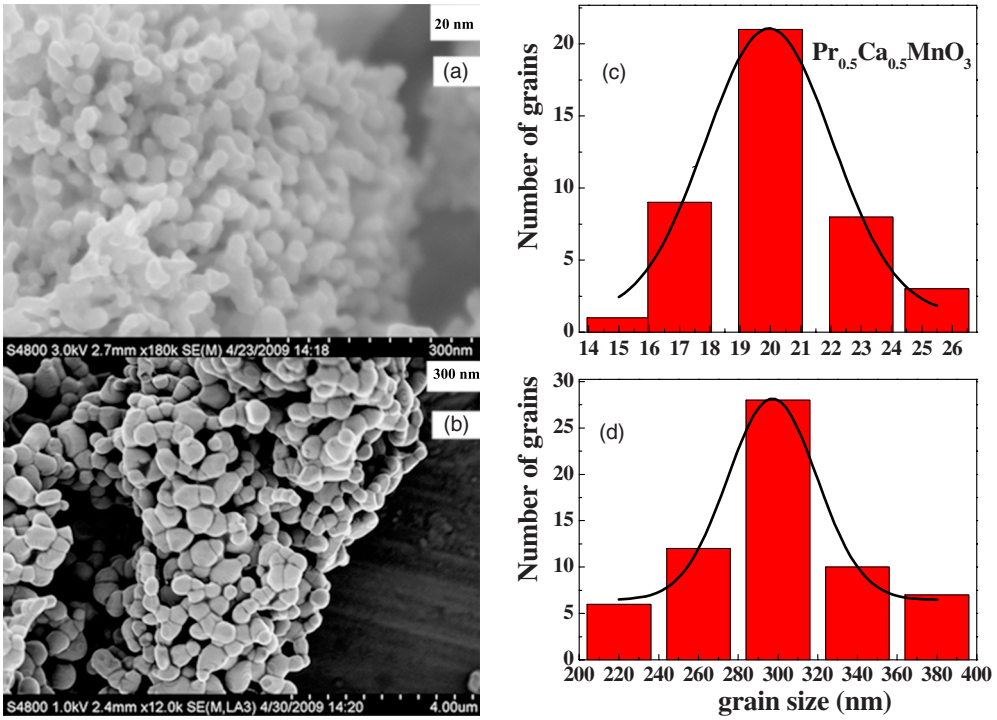

FIG. 2. (Color online) (a) The FE-SEM image and (c) the size distribution of the sample with average grain size 20 nm; (b) the FE-SEM image and (d) size distribution of the sample with average grain size 300 nm.

disappears in the M-T curves at $H=100$ Oe and only the transition to the FM or FM CG state can be seen and it becomes sharper. In order to clarify the nature of the magnetic transition (FM or FM CG phase), the magnetization relaxation was measured. In Fig. 4 the time dependence of the ZFC relaxation rate $S(t)=dM/d\ln(t)$ is shown for the sample with $D=40$ nm, the results are more in favor of the FM CG state rather than the real FM state. It is clear that $S(t)$ is dependent on the waiting time t_w, while for the FM state, $S(t)$ is independent of t_w.[31,32] Moreover, the transition temperature T_{CG} to the FM CG state, defined as the temperature corresponding to the minimum of the dM/dT, increases with decreasing grain size (Fig. 5).

The above magnetic behavior can be explained by the evolution of the spin configuration resulting from surface effects. When the bulk $Pr_{0.5}Ca_{0.5}MnO_3$ is cooled down from room temperature, it experiences a CO transition around 250 K, a CE-type AFM transition at 170 K, and then around 40 K it enters the RSG state due to the frustration caused by the competition between FM and AFM interactions.[29] For $D=300$ nm, the surface/volume ratio is very small and therefore surface effect can be neglected; accordingly, the M-T curve is very similar to that of the bulk compound.[29,30] When the particle size is reduced, the surface/volume ratio increases and the surface becomes dominant. It is known that at the surface, the electronic structure is very much different from the one in the inner core. Recently, the Monte Carlo calculations were performed for CE-type AFM/CO half-doped manganites in a three-dimensional lattice with an open surface. They indicate that the $R(A)O$ sheet termination generates an extra 0.25 electron per site at the surface.[23] The unscreened Coulomb attraction introduced at that surface enhances the charge (e_g) density on the surface (Mn layer) from 0.5 to ~0.75.[23] In perovskite manganites, the stability of the CO state is strongly related to the collinear AFM ordering of the localized Mn moments.[10,33] The enhanced itin-

TABLE I. List of the annealing temperature (T), particle size (D), width of the size distribution (w), lattice parameters (a, b, and c), and cell volume (V).

T (°C)	D (nm)	w (%)	Pr:Ca:Mn molar ratio	a (Å)	b (Å)	c (Å)	V (Å^3)
1000	300	20	1:0.96:2.05	5.406(1)	7.613(1)	5.392(1)	221.9
900	150	21	1:1.11:1.92	5.401(1)	7.596(1)	5.391 (1)	221.2
800	85	23	1:0.94:2.03	5.399(1)	7.596(1)	5.389 (1)	221.0
700	70	23	1:0.92:1.95	5.386(1)	7.564(1)	5.391(1)	219.6
600	40	24	1:1.04:1.91	5.384(1)	7.545 (1)	5.383 (1)	218.7
500	20	25	1:0.95:1.94	5.352(2)	7.531(1)	5.383(2)	217.0

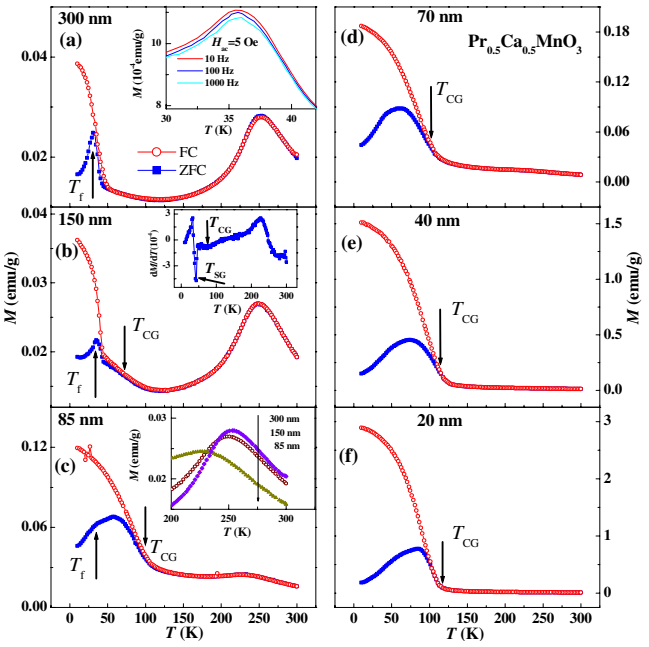

FIG. 3. (Color online) Temperature dependence of the magnetization measured in ZFC (full squares) and FC (open circles) modes at $H=100$ Oe field for the $Pr_{0.5}Ca_{0.5}MnO_3$ samples with different grain sizes. The inset of Fig. 3(a) is the ac magnetization under different frequencies for the 300 nm sample. The inset of Fig. 3(b) shows the temperature dependence of dM_{ZFC}/dT. The inset of Fig. 3(c) magnifies certain ranges of the curves for the samples with grain sizes 300, 150, and 85 nm. The difference of the T_f in dc magnetization and the T_{max} in ac magnetization in Fig. 3(a) may be because of the different measured frequency and different dc magnetic fields.

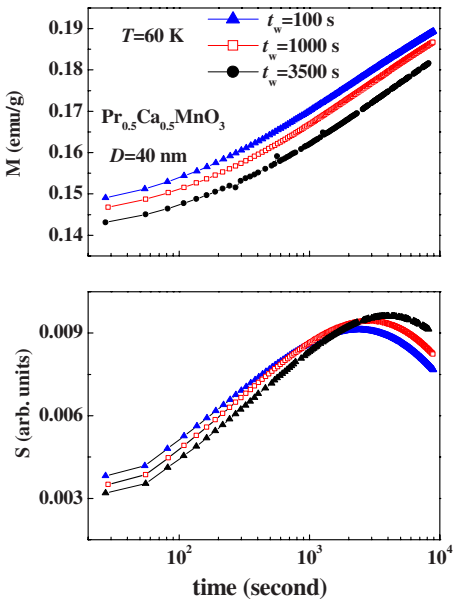

FIG. 4. (Color online) (a) ZFC relaxation magnetization and (b) corresponding relaxation rate $S(t)$ measured at $T=60$ K with different wait time as indicated for the 40-nm-sized compound $Pr_{0.5}Ca_{0.5}MnO_3$. The data were recorded at a field of $H=100$ Oe.

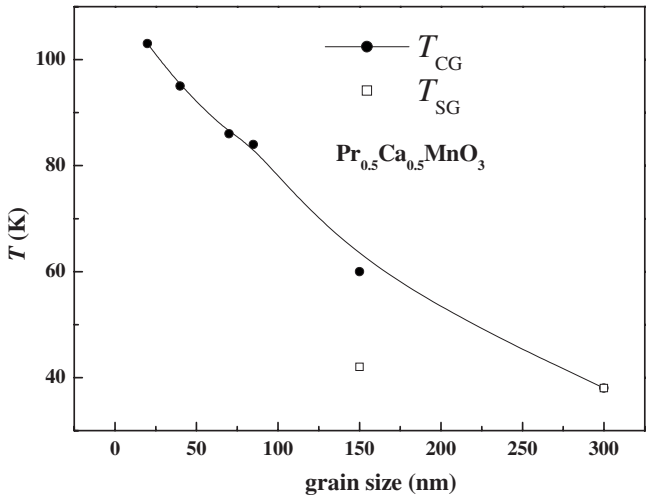

FIG. 5. Grain-size dependence of T_{SG} and T_{CG} for the compound $Pr_{0.5}Ca_{0.5}MnO_3$ with different grain sizes.

erant e_g electronic density changes the collinear AFM configuration and hence weakens the AFM superexchange coupling and improves FM double exchange interaction between Mn^{3+} and Mn^{4+} ions; thereby, the CO at the surface is suppressed. In all cases, the charge density is still 0.5 for the inner core indicating the stable CE-type AFM/CO phase. Moreover, the Monte Carlo simulations reveal that at the surface the charge distribution is inhomogeneous and electronic phase separation exists on a nanoscale.[23]

For the sample with grain size $D=150$ nm, the surface effect is still not large enough. Although the weak FM coupling caused by the enhanced charge density drives the formation of some FM clusters in the noncollinear AFM matrix at the surface, most parts of the grain are collinear AFM. Hence, only a broad upturn of the magnetization at $T\sim70$ K is observed and T_{CO} slightly decreases. The RSG state remains unchanged because the large AFM anisotropy still exists. As the grain size is further reduced, the ratio of surface/volume becomes large enough and more FM clusters appear. Furthermore, some of the FM clusters near the surface find a percolation path through the canted AFM host leading to the occurrence of the similar FM transition at higher temperature and simultaneously to the suppression of the AFM/CO state. Meanwhile, the tunneling of carriers between two Mn ions which belong to different adjacent nanoparticles also induces FM double exchange correlation.[22] Moreover, the reduction in the cell volume may also compress the Mn-O-Mn bond lengths[21] and, thus, increase the bandwidth. Therefore, FM double exchange gradually enhances and FM clusters become larger with increasing surface effects leading to a rise in T_{CG} and increasingly sharp transition. The evolution of the spin configuration is similar to that reported in Ref. 2.

From previous experimental and theoretical results[2,17,23] we know that the FM fraction is very small in nanosized AFM/CO manganites; most of phases is AFM or canted AFM. Thus, in the present measurement at $H=100$ Oe, the CO transition character may be covered up by the FM clusters for the samples with $D\leq70$ nm because the FM cluster spins are easily polarized in a small magnetic field, while the

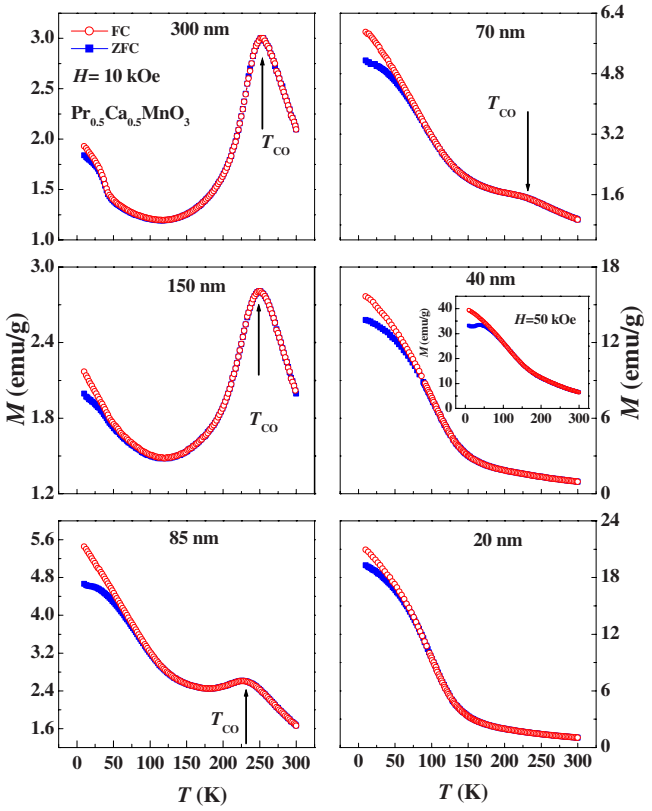

FIG. 6. (Color online) Temperature dependence of the magnetization measured in ZFC (full squares) and FC (open circles) modes at $H=10$ kOe for the $Pr_{0.5}Ca_{0.5}MnO_3$ samples with different grain sizes. The inset is the M vs T curve for the 40 nm sample measured in $H=50$ kOe.

AFM moments increase linearly with raising the magnetic field. Therefore, it is necessary to measure the M-T curves at higher magnetic fields to further clarify the charge and spin structure in nanoscale manganite $Pr_{0.5}Ca_{0.5}MnO_3$. Figure 6 shows the ZFC and FC M-T curves at $H=10$ kOe for all samples. The peak corresponding to the CO transition of the 300 and 150 nm samples obviously becomes sharper compared to those at $H=100$ Oe field. The separation between the ZFC and FC curves of the 300 nm sample almost disappears at low temperatures further supporting the RSG state. The evolution of CO peak with D is similar to that in Fig. 3. But here even for 70 nm sample CO can be distinguished, which was impossible at $H=100$ Oe. However, for samples with $D=40$ and 20 nm, this peak cannot be observed even under $H=50$ kOe, which implies the full collapse of the CO.

This behavior is very different compared to $La_{0.25(0.4)}Ca_{0.75(0.6)}MnO_3$, for which the CO state is present all the way down to grain sizes as small as 17 nm.[2,20] However, according to the Monte Carlo simulations, the charge density near the surface is enhanced, while it remains 0.5 for the inner core, i.e., the spin structure is still a stable CE-type AFM.[23] In other words the CO should exist even for very small particles. The experimental results point in the opposite direction: the CO state is completely melted below 40 nm in $Pr_{0.5}Ca_{0.5}MnO_3$. It should be noted that the theoretical model assumes that there are no frozen spins anywhere; it is done just for an individual nanograin. In fact, in our case

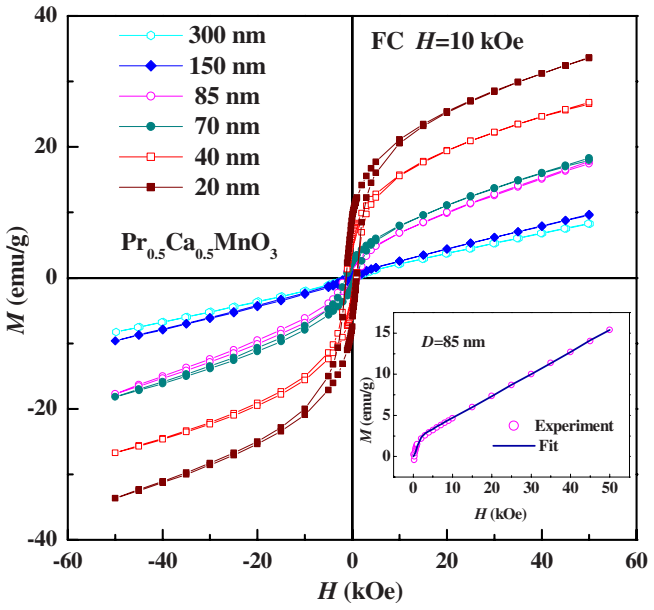

FIG. 7. (Color online) The magnetization curve M vs H measured at $T=10$ K after cooling the $Pr_{0.5}Ca_{0.5}MnO_3$ samples from room temperature in a magnetic field of $H=10$ kOe. The inset is the experimental (open circles) and fitted (solid line) results of the 85 nm sample.

there are spins frozen at low temperature, i.e., reentrant spin glass. So when the grain size is reduced below a critical value, not only do the surface spin configurations change into FM and canted AFM arrangement, but also the core spins will deviate from the collinear AFM arrangement due to the spin coupling of surface-AFM-RSG spins. On the other hand, the interparticle interaction may change the spin arrangement.[22] These facts lead to the complete collapse of the CO below 40 nm in $Pr_{0.5}Ca_{0.5}MnO_3$. While in the $La_{0.25(0.4)}Ca_{0.75(0.6)}MnO_3$ compound, CE-type and C-type AFM structures coexist,[6,34] the C-type AFM structure is much more stable than the CE-type one. Due to the spin coupling the whole magnetic structure is more stable than that in $Pr_{0.5}Ca_{0.5}MnO_3$. In addition, the large Jahn-Teller lattice distortion leads to a strong localization of doped electrons in $La_{0.25(0.4)}Ca_{0.75(0.6)}MnO_3$ compounds.[20,35] These factors prevent the CO to disappear completely above 17 nm in $La_{0.25(0.4)}Ca_{0.75(0.6)}MnO_3$ compounds.[2,20] Besides that, our case is somewhat different from the result reported by Sarkar *et al.*,[21] in which a small shoulder can be discerned in the M-T curve for the $Pr_{0.5}Ca_{0.5}MnO_3$ sample with grain size 15 nm. The upturn of the magnetization at low temperature is absent in the bulk $Pr_{0.5}Ca_{0.5}MnO_3$, while this upturn of M in $Pr_{0.5}Ca_{0.5}MnO_3$ at low temperature can be seen everywhere.[28–30,36] It is notable that if the ratio of Mn^{3+}:Mn^{4+} in $Pr_{0.5}Ca_{0.5}MnO_3$ is between 1 and 3/2 the upturn of the magnetization at low temperature is not obvious.[30] So the above behavior of their sample may result from the oxygen deficiency and their titration results also verify this deficiency.[21] Only 2 h annealing time for their bulk pellet may be responsible for the oxygen deficiency.[21]

The M-H data in Fig. 7 further support the above analysis. For the smaller grain sizes, the hysteresis becomes more pro-

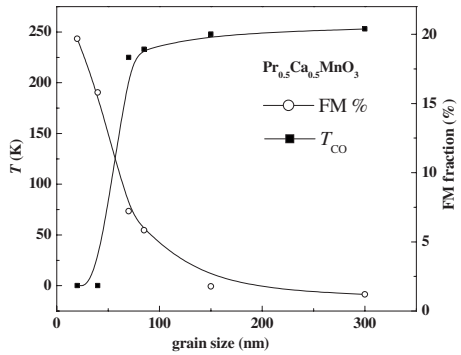

FIG. 8. Grain-size dependencies of the charge-order transition temperature T_{CO} (full squares, left axis) and ferromagnetic fraction (open circles, right axis) for compound $Pr_{0.5}Ca_{0.5}MnO_3$.

nounced and the magnetization at $H=50$ kOe monotonously increases with decreasing grain size. Three stages can be distinguished as the particle size is reduced: (i) for the 300 and 150 nm samples, the surface effects are not obvious and the weak FM interaction results in a small magnetization; (ii) for $D=85$ and 70 nm, the CO is significantly weakened and the FM coupling is much more pronounced compared to $D=300$ and 150 nm. This leads to a significantly larger magnetization; (iii) for the 40 and 20 nm samples, the CO is completely suppressed and the full collinear AFM configuration is changed by spin coupling; thus, their magnetization is much larger than the one observed in 85 and 70 nm samples. This trend becomes clearer from Fig. 8 where T_{CO} and the FM cluster fraction are displayed as a function of grain size. Here the FM fraction is calculated using $M_{S,10\ K}/M_{ideal}$ ($M_{ideal}=3.5\ \mu_B$/f.u. assuming full FM alignment of the spins for $Pr_{0.5}Ca_{0.5}MnO_3$) and the spontaneous magnetization M_S is determined by $M(H)=M_S[1-a/H-b/H^2]+\chi_d H$, where $\chi_d H$ is the high-field differential susceptibility and a and b are fit parameters.[37] As an example, the fitted result of the 85 nm sample is shown in the inset of Fig. 7. Both T_{CO} and the FM cluster fraction show a sharp variation when $D \leq 70$ nm.

The weakness of the AFM/CO state in nanosized $Pr_{0.5}Ca_{0.5}MnO_3$ is also confirmed by the magnetic field effect on the CO. Figure 9 shows the temperature dependence of the magnetization for $D=85$ nm at different magnetic fields. As the field strengthens, the CO peak first becomes sharper and then weak. Eventually it completely disappears at a magnetic field of $H=60$ kOe. In contrast, for the bulk compound $Pr_{0.5}Ca_{0.5}MnO_3$, the CO state does not collapse completely until the magnetic field reaches $H=270$ kOe.[10] In addition, the difference between FC and ZFC magnetization at low temperatures first becomes smaller when the magnetic field increases from $H=100$ Oe, but then increases around $H=10$ kOe. The onset temperature of the difference defined as the irreversibility temperature T_{irr} also shows the same evolution. The first increase from $H=100$ to 10 kOe is easily understood since at low temperatures, FM cluster spins freeze into random orientation dictated by the local anisotropy field. Since the $H=100$ Oe field is not strong enough to overcome the local anisotropy field, the ZFC magnetization is much lower than the FC one with the FM spins

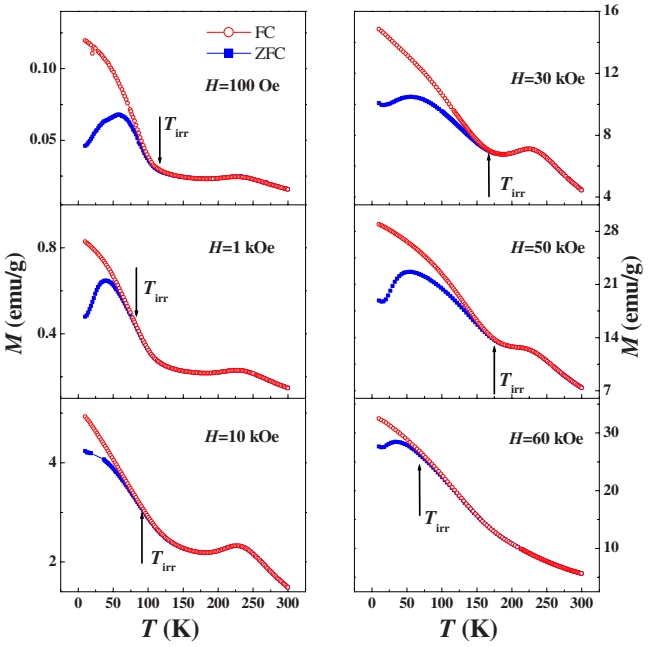

FIG. 9. (Color online) FC (open circles) and ZFC (full squares) magnetization M versus T curves for 85-nm-sized $Pr_{0.5}Ca_{0.5}MnO_3$ sample under different magnetic fields.

aligned upon FC. Upon raising external fields, the local anisotropy field can be overruled and the FM spins align, which make the difference vanish between the ZFC and FC states. The difference becomes larger again when the magnetic field rises from $H=10$ to 50 kOe, which is similar to the previous data.[38,39] At these high fields, upon FC more spins deviate from the collinear AFM arrangement, inducing the weak FM coupling, compared to the case of ZFC.[38] The difference is particularly large due to the existence of the phase separation.[38,39] At $H=60$ kOe, all spins deviate from the robust collinear AFM configuration observed in bulk compounds. This leads to the disappearance of the CO and to a significant decrease in the difference of FM spins between the FC and the ZFC processes, which leads to small difference only at low temperatures.

Since the FM clusters and AFM phase coexist in nanosized $Pr_{0.5}Ca_{0.5}MnO_3$ and the FM fraction increases with reducing particle size, one can expected the EB and a size modulation of the EB. In Fig. 10 the hysteresis loops are plotted for $Pr_{0.5}Ca_{0.5}MnO_3$ samples with different particle sizes; the measurements have been done at $T=10$ K in both ZFC and FC modes. In the FC process the hysteresis loops shift toward the negative fields and the positive magnetization, exhibiting the EB behavior. In contrast, the loops are still centered about the origin in the ZFC case. The coexistence of the FM clusters and AFM phase leads to the natural FM/AFM interfaces as the sample is cooled down to $T=10$ K at $H=10$ kOe external field. The spins of the FM cluster align parallel to the external magnetic field. The interfacial FM spins on the exterior surface of the AFM or canted AFM inner core tend to be coupled with AFM spins at the interface as the temperature is below T_N; this leads to the EB behavior. The EB field H_{eb} is generally defined as $H_{eb}=|H_1+H_2|/2$ and the coercivity is given by $H_C=|H_1-H_2|/2$,

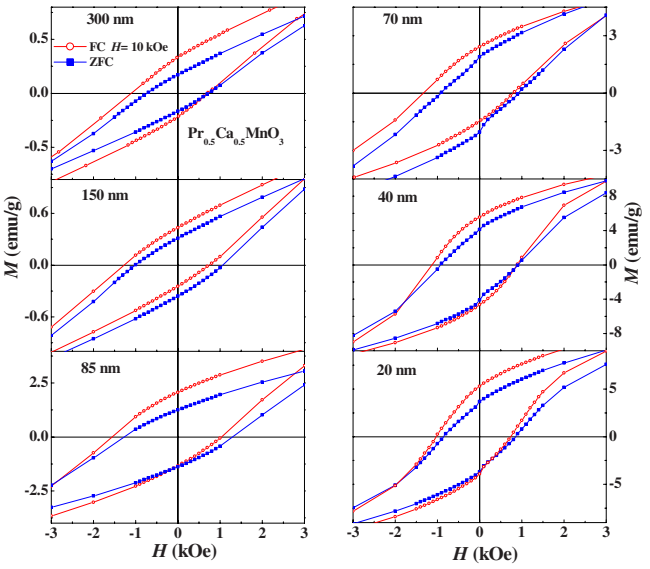

FIG. 10. (Color online) The magnetic field dependence of the magnetization at $T=10$ K after the $Pr_{0.5}Ca_{0.5}MnO_3$ samples are cooled down to $T=10$ K from room temperature in FC (open circles) under $H=10$ kOe field and ZFC (full squares) procedures for all the samples with different grain sizes.

where H_1 and H_2 are the left and right coercive fields, respectively. The remanence asymmetry M_{eb} corresponds to the shifts in the vertical magnetization; it is defined as $M_{eb}=|M_1+M_2|/2$, where M_1 and M_2 are the positive and negative remanent magnetization, respectively. In order to get some insight into the sized effects on the EB, in Fig. 11 the size-dependent EB parameters H_{eb}, H_C, M_{eb}, and M_{eb}/M_s are plotted. It can be seen that all the parameters show a nonmonotonic evolution with decreasing grain size and demonstrate a maximum at about 85 nm. The EB effect in our case is much larger than that in $La_{0.7}Ca_{0.3}MnO_3$ nanoparticles with FM core and spin-glass shell, for which, the EB effect is only found in the 24 nm sample and it disappears in the 39 nm sample.[26]

It is well known that the EB originates from the spin coupling at FM/AFM interface. In FM/AFM bilayer films, the H_{eb} is not only related to the FM layer thickness but also related to the thickness of the AFM layer.[24,25] Here, for the $Pr_{0.5}Ca_{0.5}MnO_3$ nanoparticles, the rise in the charge density drives the surface layer from an AFM/CO state to FM clusters and canted AFM phase-separated state; the FM fraction increases, albeit, the FM layer thickness is almost constant with decreasing grain size.[40] This increases the number of FM/AFM interface and thereby enhances the exchange energy at the interfaces; eventually it leads to the increase in H_{eb}. But we must keep in mind that in addition to the exchange energy, there are two other energy terms contributing to the EB: the effective Zeeman energy of the FM component and the anisotropy energy of the AFM core.[25] With decreasing particle size, the thickness, (i.e., the volume of the AFM core) becomes gradually smaller, which leads to a reduction in the anisotropy energy of the AFM core ($E_A \sim KV$, where K is the anisotropy constant and V is the volume of the core). Hence, the pinning energy of the AFM spins to FM spins becomes weaker and the FM spins are

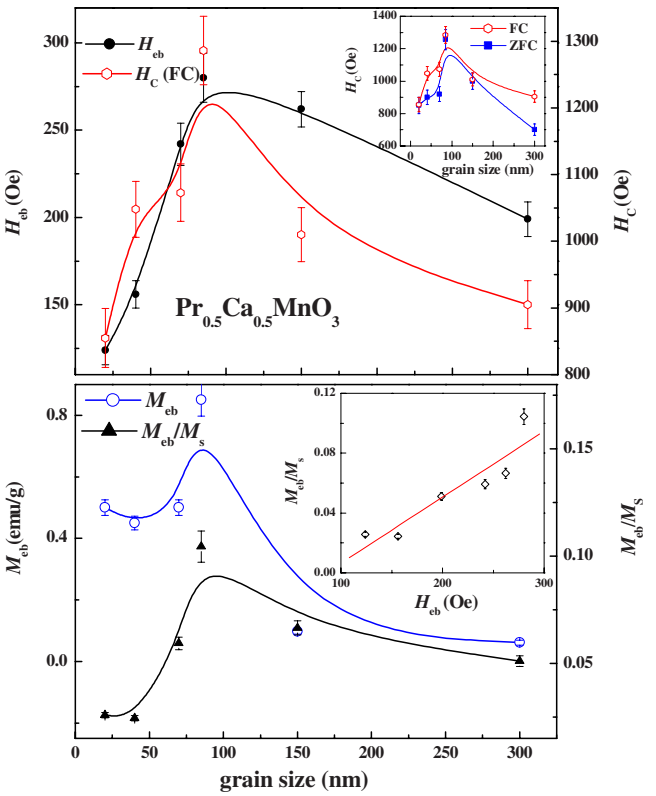

FIG. 11. (Color online) Grain-size dependencies of the H_{eb}, H_C, M_{eb}, and M_{eb}/M_s of compound $Pr_{0.5}Ca_{0.5}MnO_3$ at $T=10$ K. The inset of (a) is the grain-size dependences of FC and ZFC H_C at $T=10$ K. The inset of (b) shows H_{eb} as a function of M_{eb}/M_s at $T=10$ K.

easily reversed by magnetic field reducing the value of H_{eb}. One the other hand, the growth of the FM fraction increases the Zeeman energy, which also weakens the EB field.[25] Therefore, when the two competitive factors reach a balance, the H_{eb} exhibits a maximum. Thereafter, with further diminishing grain size, the latter factor dominates and causes a reduction in H_{eb}. As for the coercivity, the increasing FM fraction strengthens the spin coupling at the FM/AFM interface with decreasing grain size, which equally enlarges the anisotropy of the FM component and leads to the rise in the coercivity H_C. Meanwhile the diminished anisotropy energy of the AFM core weakens the pinning of the AFM spins to FM spins at the interface and result in a reduction of H_C. Additionally, the more prominent the thermal fluctuations, the smaller the particle size, which also reduce the FM anisotropy.[41] When these competing factors balance each other, the peak appears in the curve H_C versus grain size. The enhanced H_C observed in the FC process, as shown in the inset of the Fig. 11(a), is usually attributed to the largely enhanced unidirectional anisotropy of FM clusters in the FM/AFM interface.[24] A simple close-linear correlation between H_{eb} and M_{eb}/M_S [see the inset of the Fig. 11(b)], as reported by Huang *et al.*[27] and Niebieskikwiat *et al.*,[41] indicates a close correspondence of both parameters, implying the same origin.[41]

Our results suggest that the CO and EB in the nanosized manganites can be effectively tuned by the particle size. It

means that this type of tunable charge ordering and exchange bias arises from the sensitivity of order parameters to geometry and size in strongly correlated materials. These results have an important implication for the development of nanomultifunctional spintronic devices and systems.

IV. CONCLUSION

In summary, the influence of the grain size on the CO and EB was investigated in CE-type AFM/CO $Pr_{0.5}Ca_{0.5}MnO_3$. The increase in the charge density (e_g electron) at the surface of the nanoparticles drives the surface layer from a CO state with collinear AFM configuration to the coexistence of the charge-disordered canted AFM and FM states. Reducing the particle size, surface effects dominate and suppress the CO. When the grain size is reduced below 40 nm, CO completely melts because the core spin configuration changes from antiparallel arrangement to canted AFM through spin coupling. At the same time, the enhanced FM spin coupling increases the FM fraction. The EB field H_{eb} and the coercivity H_C show a nonmonotonic behavior with diminishing the particle size. This can also be understood in the light of the evolution of the spin configuration. These results are helpful to further understand the role of the spin configuration in the AFM/CO manganites.

ACKNOWLEDGMENTS

We thank B. Gompf, G. Untereiner, and J. Elling for their assistance. T. Zhang acknowledges support by the Alexander von Humboldt Foundation.

[1] *Colossal Magnetoresistive Oxides*, edited by Y. Tokura (Gordon and Breach, Tokyo, 1999).
[2] T. Zhang, T. F. Zhou, T. Qian, and X. G. Li, Phys. Rev. B **76**, 174415 (2007).
[3] C. Sen, G. Alvarez, and E. Dagotto, Phys. Rev. Lett. **98**, 127202 (2007).
[4] S. Cox, E. Rosten, J. C. Chapman, S. Kos, M. J. Calderon, D. J. Kang, P. B. Littlewood, P. A. Midgley, and N. D. Mathur, Phys. Rev. B **73**, 132401 (2006).
[5] S. Dong, H. Zhu, and J. M. Liu, Phys. Rev. B **76**, 132409 (2007).
[6] M. Pissas and G. Kallias, Phys. Rev. B **68**, 134414 (2003).
[7] T. S. Orlova, J. Y. Laval, P. Monod, J. G. Noudem, V. S. Zahvalinskii, V. S. Vikhnin, and Y. P. Stepanov, J. Phys.: Condens. Matter **18**, 6729 (2006).
[8] D. P. Kozlenko, Z. Jirák, I. N. Goncharenko, and B. N. Savenko, J. Phys.: Condens. Matter **16**, 5883 (2004).
[9] C. W. Cui and T. A. Tyson, Phys. Rev. B **70**, 094409 (2004).
[10] M. Tokunaga, N. Miura, Y. Tomioka, and Y. Tokura, Phys. Rev. B **57**, 5259 (1998).
[11] T. Zhang, G. Li, T. Qian, J. F. Qu, X. Q. Xiang, and X. G. Li, J. Appl. Phys. **100**, 094324 (2006).
[12] P. Dey and T. K. Nath, Appl. Phys. Lett. **87**, 162501 (2005).
[13] M. L. Moreira, J. M. Sores, W. M. de Azevedo, A. R. Rodrigues, F. L. A. Machado, and J. H. D. Araujo, Physica B **384**, 51 (2006).
[14] A. I. Shames, M. Auslender, E. Rozenberg, E. Sominski, A. Gedanken, and Ya. M. Mukovskii, J. Appl. Phys. **103**, 07F715 (2008).
[15] M. H. Zhu, Y. G. Zhao, W. Cai, X. S. Wu, S. N. Gao, K. Wang, L. B. Luo, H. S. Huang, and L. Lu, Phys. Rev. B **75**, 134424 (2007).
[16] V. Markovich, I. Fita, A. Wisniewski, R. Puzniak, D. Mogilyansky, L. Titelman, L. Vradman, M. Herskowitz, and G. Gorodetsky, Phys. Rev. B **77**, 054410 (2008).
[17] S. S. Rao, S. Tripathi, D. Pandey, and S. V. Bhat, Phys. Rev. B **74**, 144416 (2006).
[18] C. L. Lu, S. Dong, F. Gao, Z. Q. Wang, J. M. Liu, and Z. F. Ren, Appl. Phys. Lett. **91**, 032502 (2007).
[19] T. Sarkar, B. Ghosh, A. K. Raychaudhuri, and T. Chatterji, Phys. Rev. B **77**, 235112 (2008).
[20] E. Rozenberg, M. Auslender, A. I. Shames, D. Mogilyansky, I. Felner, E. Sominskii, A. Gedanken, and Ya. M. Mukovskii, Phys. Rev. B **78**, 052405 (2008).
[21] T. Sarkar, P. K. Mukhopadhyay, A. K. Raychaudhuri, and S. Banerjee, J. Appl. Phys. **101**, 124307 (2007).
[22] E. Rozenberg, A. I. Shames, M. Auslender, G. Jung, I. Felner, J. Sinha, S. S. Banerjee, D. Mogilyansky, E. Sominski, A. Gedanken, Ya. M. Mukovskii, and G. Gorodetsky, Phys. Rev. B **76**, 214429 (2007).
[23] S. Dong, R. Yu, S. Yunoki, J. M. Liu, and E. Dagotto, Phys. Rev. B **78**, 064414 (2008).
[24] J. Nogues and Ivan K. Schuller, J. Magn. Magn. Mater. **192**, 203 (1999).
[25] J. Nogués, J. Sort, V. Langlais, V. Skumryev, S. Surinach, J. S. Munoz, and M. D. Baró, Phys. Rep. **422**, 65 (2005).
[26] M. Muroi, P. G. McCormick, and R. Street, Rev. Adv. Mater. Sci. **5**, 76 (2003).
[27] X. H. Huang, J. F. Ding, G. Q. Zhang, Y. Hou, Y. P. Yao, and X. G. Li, Phys. Rev. B **78**, 224408 (2008).
[28] Z. Jirák, F. Damay, M. Hervieu, C. Martin, B. Raveau, G. André, and F. Bourée, Phys. Rev. B **61**, 1181 (2000).
[29] G. X. Cao, J. C. Zhang, S. P. Wang, J. Yu, C. Jing, S. X. Cao, and X. C. Shen, J. Magn. Magn. Mater. **301**, 147 (2006).
[30] M. R. Lees, J. Barratt, G. Balakrishnan, D. McK. Paul, and C. D. Dewhurst, J. Phys.: Condens. Matter **8**, 2967 (1996).
[31] D. N. H. Nam, K. Jonason, P. Nordblad, N. V. Khiem, and N. X. Phuc, Phys. Rev. B **59**, 4189 (1999).
[32] H. Woo, T. A. Tyson, M. Croft, and S. W. Cheong, J. Phys.: Condens. Matter **16**, 2689 (2004).
[33] R. Y. Gu, Z. D. Wang, and C. S. Ting, Phys. Rev. B **67**, 153101 (2003).
[34] M. Pissas, I. Margiolaki, K. Prassides, and E. Suard, Phys. Rev. B **72**, 064426 (2005).
[35] X. G. Li, R. K. Zheng, G. Li, H. D. Zhou, R. X. Huang, J. Q. Xie, and Z. D. Wang, Europhys. Lett. **60**, 670 (2002).
[36] B. Raveau, A. Maignan, and C. Martin, J. Solid State Chem. **130**, 162 (1997); K. Vijaya Sarathy and P. Sreeraj, Solid State

Commun. **122**, 385 (2002); L. Pi, E. Fan, Y. Z. Zhang, J. X. Ma, S. Tan, and Y. H. Zhang, J. Magn. Magn. Mater. **314**, 87 (2007); S. Nair and A. Banerjee, Phys. Rev. Lett. **93**, 117204 (2004); S. S. Rao, K. N. Anuradha, S. Sarangi, and S. V. Bhat, Appl. Phys. Lett. **87**, 182503 (2005).

[37] J. Fontcuberta, B. Martínez, V. Laukhin, Ll. Blacells, X. Obradors, C. H. Cohenca, and R. F. Jardim, Philos. Trans. R. Soc. London, Ser. A **356**, 1577 (1998).

[38] T. Qian, G. Li, T. Zhang, T. F. Zhou, X. W. Kang, and X. G. Li, Phys. Rev. B **76**, 014433 (2007).

[39] R. Mahendiran, A. Maignan, C. Martin, M. Hervieu, and B. Raveau, Phys. Rev. B **62**, 11644 (2000).

[40] L1. Balcells, J. Fontcuberta, B. Martinez, and X. Obradors, Phys. Rev. B **58**, R14697 (1998).

[41] D. Niebieskikwiat and M. B. Salamon, Phys. Rev. B **72**, 174422 (2005).